Evaluating Individual mRNA Molecules Detection Techniques in Microscope Images

Rethabile Khutlang, Loretta Magagula, Musa Mhlanga
Gene Expression and Biophysics Group
Emerging Health Technologies
CSIR Biosciences
Pretoria, South Africa
rkhutlang@csir.co.za

***Abstract*—Single molecule fluorescence *in situ* hybridization followed by microscopic image analysis is one of the prominent methods used to study gene expression on a single cell level. There are various microscopic image analysis methods, leading to differing mRNA spots being detected in images for the same experiment. We present a technique to evaluate different mRNA spots detection algorithms. It is based on image annotation by expert biologists and the receiver operating characteristics. The detection methods can be compared using parameters that withstand imprecise and imbalanced environments. The proposed evaluation procedure highlighted the difference between two microscopic image analysis methods that are frequently used. It can be applied to any image analysis method that seeks to find mRNA spots on a single cell level.**

Keywords—sm-FISH; spot detection; receiver operating characteristics; F-measure

I. BACKGROUND

Gene expression is studied more and more on the single cell level [1]. One of the methods used to provide mRNA counts in individual cells is single molecule fluorescence *in situ* hybridization (sm-FSIH) followed by microscopic image analysis [2].

Single molecule FISH is a microscopy-based assay that allows for the visualization, detection and localization of specific nucleic acid sequences in their native environment. Since its origins, over 20 years ago [3], it has become a powerful molecular tool for the detection of cytogenetic and molecular genetic alterations. Applications of FISH have even extended to clinical diagnosis – chromosome analysis [4]. In a molecular setting, FISH has revealed insights in transcriptional dynamics [5, 6], mechanisms of RNA synthesis [2] and transport [7] and intracellular distribution [8,9].

The first application of fluorescent *in situ* detection involved the use of RNA probes directly labelled on the 3'end with a fluorophore to bind specific DNA sequences [10]. The labelling of probe sequences developed to use fluorophore-coupled amino-allyl modified bases [11] and the use of enzymatic incorporation of fluorophore-modified bases [12]. These advances in the technology allowed for the simple chemical production of an array of low-noise probes. Attempts to improve signal output of this assay came in the form of nick-translated, biotinylated probes, which were indirectly detected using fluorescently labelled streptavidin conjugates [13]. Currently, the standard FISH probe is produced by simple esterification chemistry to couple fluorophore to a 3'amine-modified base [14]. This method of probe preparation allows for precise and direct detection with high signal-to-noise ratios, improving the sensitivity of the assay.

Initially, RNA detection using FISH was constrained to use of large oligonucleotide probes. This was problematic as large probes could adhere to samples non-specifically resulting in false positives as well as lead to high levels in background noise. The use of reduced probe sizes lead to improved signal-to-noise-ratio and sensitivity, allowing for the single-copy detection of RNA entities and even parts of RNA [15, 16]. In this variation of the assay, 5 oligonucleotides, each about 50 oligonucleotides long, were labelled with fluorophore moieties. The hybridization of these probes to their mRNA targets yielded each target to be visualized as a diffraction-limited fluorescent "spot" [16]. However, the synthesis and purification of a small number of heavily labelled probes came with high difficulty and these probes tended to interact with each other altering hybridization characteristics which lead to severe quenching [17]. An improvement of the assay was made by using a tandem array (12-48) of reliably and singly labelled probes to accurately detect individual mRNA molecules at high spatial-temporal resolution. This advancement in the assay has lead to the simultaneous and accurate detection of multiple targets using spectrally distinct fluorophores within the same sample [18,19].

Post image acquisition, Femino et al. [16] used a constrained deconvolution algorithm to quantitatively restore out-of-focus light to its original points of origin. They could then calibrate for the fluorescent output per molecule of probe. In [19], calibration of fluorescent output per molecule of probe was not performed, however for 48 probes per mRNA they detected the same number of mRNA spots per image over a broad range of thresholds, validating the choice of a threshold parameter. Additionally, they avoided the difficulty in synthesizing and purifying heavily labelled probes.

Raj et al. [19] used the Laplacian of Gaussian filter to remove the non-uniform background and enhance particles. The resulting image conserves spatial resolution of spots, so

does the wavelet transform based filtering as used in [20]. The procedures are computationally less expensive than constrained deconvolution algorithms; so is the procedure proposed by Trcek et al. [21] – spatial band-pass filtering and local background subtraction to remove residual unevenness in the image.

There are different thresholding techniques that are applied to a filtered image to eventually find spots [16,19,20,21]. Raj et al. [19] chose a threshold from a range of thresholds for which the number of mRNAs detected varied the least. Trcek et al. [21] used Gaussian mask fitting to find the centre and intensity of each spot. In any case, the detected spots can be analysed on a per cell basis if the cell marker is used in an experiment.

We present an evaluation of individual mRNA molecules detection techniques in microscope images. The evaluation procedure is applied to two detection techniques. It is based on the use of expert biologists as the gold standard in marking spots in a microscope image. The evaluation procedure uses the receiver operating characteristics analysis (ROC) and performance evaluation metrics used in machine vision and learning.

The organisation of this paper is as follows. The next section outlines the method of evaluating detection techniques (methods used to prepare mRNAs are in supplementary data). Then detection techniques evaluation results are presented.

II. METHODS

A. Spots validation

Spots found in a z-stack image by an expert biologist constituted the gold standard used in evaluating the performance of a detection algorithm on that stack. Biologists circled all mRNA spots they could find using a custom made GUI. Hausdorff distance [22] was used to study intra- and inter-observer variability in marking spots and compare that to detection algorithms' found spots; the modified Williams index (MWI) [23] was obtained from the Hausdorff distances to further compare algorithms' spots boundaries to hand drawn ones. The index is the ratio between the average computer-observer agreement and the average observer-observer agreement. For N observations, MWI is calculated leaving one observation out at a time, for N-1 observations, resulting in N estimates.

B. Detection techniques evaluation

The posterior probability of a detected spot was calculated by finding the ratio of pixels found by both an algorithm and an expert to pixels found by an expert; minus fraction of pixels missed or over-segmented by an algorithm. Background pixels were regarded as non-target objects. The ROC curves were plotted using spots as the target class. The area under the ROC curve (AUC) is used as an evaluation value integrating the entire ROC. Sensitivity and specificity, typical two-class detection performance evaluation measures, could be established from the ROC curve at a chosen operation point.

Since the non-target class far exceeds the target class, the posfrac-recall ROC [24,25] was used to evaluate detection algorithms, as this is the imbalanced problem. The prior probability of the positive class is significantly less than that of the negative class, their ratio – skew, was used to study what fraction of non-target objects to include in the analysis. Typical imprecise environment detection evaluation measures can then be used to compare detection algorithms at one operating point: posfrac – fraction of positive detections (1),

$$posfrac = \frac{TP + FP}{N} \tag{1}$$

precision (2) – the fraction of positive detections that are actually correct and it is usually a meaningful parameter when detecting rare events because it effectively estimates an overall posterior probability [25],

$$precision = \frac{TP}{TP + FP} \tag{2}$$

recall and F-measure (3) – the geometric mean of precision and recall [25]. TP denotes the test objects labeled as target and are truly targets, while FP denotes false targets. TP_r - recall, and FP_r are calculated by normalizing TP and FP by the total number of positive and negative objects respectively, N is the sum of positive and negative objects. TP_r indicates sensitivity while 1 – FP_r denotes specificity.

$$F - measure = 2TP_r \frac{2TP_r}{TP_r + FP_r + 1} \tag{3}$$

III. RESULTS

A. Spot validation

Spot validation was studied using a set of 10 z-stack images. In each stack, the plane that showed spots the most clearly was chosen. The similarity of spots marked by the two expert biologists was studied on spots contours extracted using the custom made GUI. The comparisons in Table I were made using the Hausdorff distance. T11 and T12 represent the first expert marking spots the first and second times, more than a week apart, T2 represents the second expert. AL1 represents spots detected using the image analysis procedure outlined in [19], while AL2 represents spots found using wavelets-based detector [20].

The first expert had the highest intra-observer variability, 4.5518. There was the highest dissimilarity in the ellipses drawn around spots. The variability is further confirmed by the standard deviation of the Hausdorff distances between the first and second times the first expert marked the spots, it is the highest. The second expert still had high intra-observer variability, although it was not higher than inter-observer variability. The standard deviation of inter-observer variability is the second highest, elucidating the difference in marking spots between the two experts.

The mean Hausdorff distances between first round of spot marking by experts and automated detection procedures were lower than those between and among experts; prompting a

TABLE I. COMPARISON OF SPOTS MARKED BY TWO EXPERTS AND THOSE FOUND BY LOG PLUS THRESHOLDING AND WAVELETS BASED-METHODS

	T11& T12	T21& T22	T11& T21	T11& AL1	T21& AL1	T11& AL2	T21& AL2
Mean	4.5518	4.4353	4.5190	4.2816	4.1721	4.2768	4.1102
Std	1.5064	1.1813	1.4060	1.3628	1.0184	1.3247	1.1138

TABLE II. COMPARISON OF SPOTS MARKED BY THE TWO EXPECTS THE SECOND TIME AND THOSE FOUND BY LOG PLUS THRESHOLDING AND WAVELETS BASED- METHODS

	T12&AL1	T22&AL1	T12&AL2	T22&AL2
Mean	4.5932	4.1684	4.5353	4.1472
Std	1.0878	1.1322	1.1336	1.1209

suspicion than maybe experts marked spots differently the second time, a week later. The Hausdorff distances between both LoG-based and wavelets-based detections and experts the second time they marked spots were calculated, Table II.

Instead of experts marking spots differently the second time, Table II suggests that the first expert has higher variability in marking spots than the second expert. This is because variability between the second expert marking spots the second time and automated detections is stable when compared to that expert the first time and automated detections. This observation suggests that the first expert is the source of variability. The low Hausdorff distances between the first expert the first time and automated detections imply that though the first expect had the highest overall variability, the first expert had high variability the second time they marked spots.

Table II further shows that spot contours found by the wavelets-based method agree better with experts than those found using LoG-based method, as this was established in Table I. Fig. 1 shows typical spots marked by the first expert side by side with those detected by the two methods. If the first expert had the highest variability in marking the spots, yet visually that expert's spots marking look consistent then it can be concluded that the two experts marked spots similarly. Spots detected by automated detections visually have contours that differ from those of experts, however are acceptable as Hausdorff distances for 10 stacks are comparable to those of inter-expert.

The set of expert markings comprised four observations per object; two experts marked spots twice. The value of the MWI for the LoG based method was 1.0094; its 95% confidence interval, assuming the standard normal distribution, was (1.0070, 1.0118). The value of the MWI for the wavelets based method was 1.0172; its 95% confidence interval was (1.0148, 1.0196). The upper limit of the confidence interval for both methods is greater than one, indicating that the methods agree with the experts at least as well as the experts agree with each other.

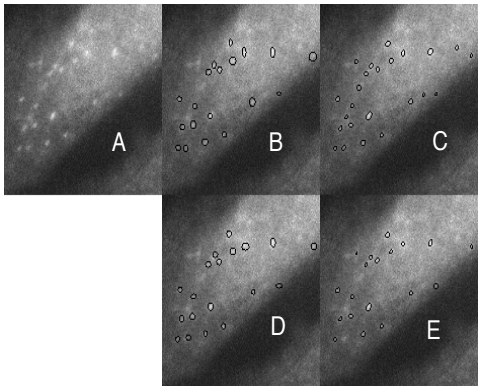

Figure 1. A shows original image, B is spots marked by the first expert the first time, C highlights those detected by the LoG-based method, D shows spots marked by the expert the second time and lastly E is spots found using wavelets-based method.

B. Detection techniques evaluation

Fig. 2 shows ROC plot for both methods using objects on a z-stack level deemed the most in focus visually. Spots marked by an expert constituted the gold standard. The AUC for the LoG-based method was 0.7751, while that of the wavelets-based method was 0.6070. The LoG-based method had a higher AUC value; over a range of posterior probabilities cut-offs it had better performance than the wavelets-based method.

For each method, at the operating point corresponding to posterior probability threshold set at 0.5, Table III shows the performance evaluated using parameters deemed suitable for imprecise environment. Sensitivity versus specificity was considered not informative enough, as the two classes were imbalanced.

Even though the LoG-based method had the highest AUC value, it is less precise than the wavelets-based method at the operating point chosen. Precision, what fraction of detected spots are actually spots should be an important measure in evaluating detection algorithms as noise frequently increases the false positive detections. The gain in precision came at the loss in sensitivity – recall. Sensitivity fell by 10% for an increase in precision of 20.50%. The wavelets-based method picks up a lot less non-spots, a quarter of those by LoG-based method, objects at the expense of missing a few true positive spots. This leads to the implication that maybe the normal ROC is not suitable for this problem; the posfrac-recall ROC could offer better performance evaluation.

TABLE III. PERFORMANCE EVALUATION OF THE LOG-BASED AND WAVELETS-BASED METHODS THE IN THE IMPRECISE ENVIRONMENT

	Precision	Recall	F-measure	Posfrac
LoG-based	0.6906	0.9600	0.6575	0.9720
Wavelets-based	0.8958	0.8600	0.6324	0.8727

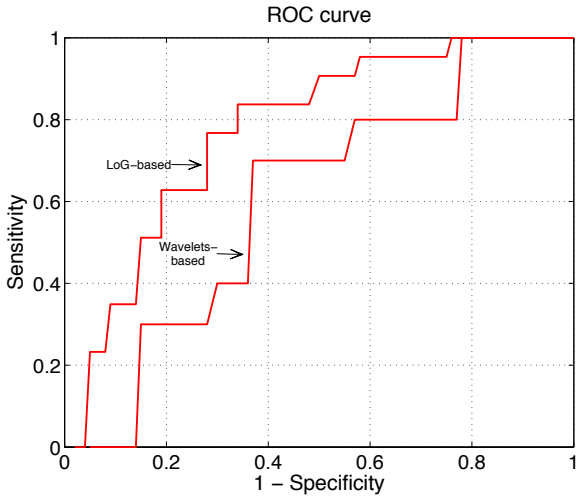

Figure 2. Example The ROC curves for the LoG-based and wavelets-based methods.

Figures 3 and 4 show posfrac-recall ROC curves for the LoG-based and wavelets-based methods respectively, for the target prior probabilities π_t= 0.5, 0.1 and 0.01. The prior probability of the non-target class was varied by varying the fraction of background pixels from the gold standard image considered as the non-target objects.

The posfrac-recall curves indicate that the two methods have similar performance with varying skew values. The choice of skew, fraction of non-target objects to include in evaluating a method, depends on the percentage of posfrac deemed acceptable in detecting spots in an application. The posfrac of both methods lowers with increasing skew for a set sensitivity. However, precision is fixed as skew varies.

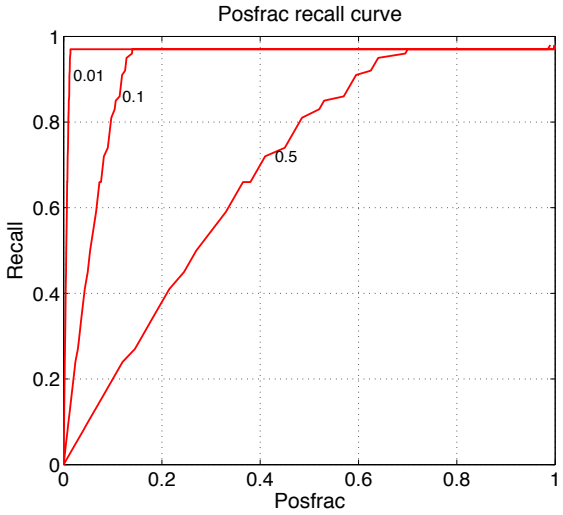

Figure 3. The posfrac-recall ROC curves for the LoG-based method.

TABLE IV. POSFRAC OF THE LOG- AND WAVELETS-BASED METHODS FOR VARYING VALUES AT 80% SENSITIVITY AND THEIR AUC VALUES

π_t	LoG		Wavelets	
	AUC	Posfrac	AUC	Posfrac
0.5	0.6844	0.4800	0.6524	0.4350
0.1	0.9129	0.0960	0.8425	0.0870
0.01	0.9643	0.0096	0.8852	0.0087

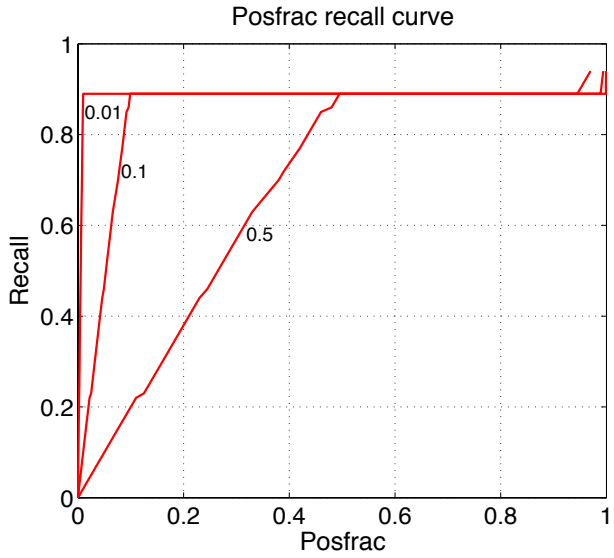

Figure 4. The posfrac-recall ROC curves for the wavelets-based method.

According to posfrac-recall curves, the LoG-based method has better overall sensitivity; but since it is less precise than the wavelets-based method its posfrac is high due to high false positives. Table 4 shows the posfrac of the two methods at 80% sensitivity with varying skew; it also shows their AUC. At 80% sensitivity, the wavelets-based method has lower posfrac for all skew values.

However, above maximum sensitivity of the wavelets-based method, its posfrac significantly surpasses that of the LoG-based method. That is confirmed by the AUC values – LoG-based method values are consistently higher than those of the wavelets-based method. The choice of the skew value and sensitivity at which to operate depends on the problem being investigated. If a method that finds all the spots, even at an expense of including background noise is desired, the high posfrac value can be ignored.

When the spot detection algorithms performance evaluation is treated as an imbalanced case problem, the posfrac-recall curves can be used to help decide at what skew and sensitivity different methods can be compared. This is appropriate because the distribution of spots to be detected is not known a priori. The methods are evaluated on a per stack basis, but the evaluations can be conducted on a batch of stacks of images. Spots can be detected in 3D or maximum projections of stacks, the evaluation metrics proposed would still hold. The

evaluation metrics can be applied to other spot detection algorithms, not just the two tested here.

IV. CONCLUSIONS

We have proposed a procedure to evaluate performance of spot detection algorithms in microscope images. The procedure depends on the marking of spots in images by an expert biologist. The marked spots form a gold standard in determining accuracy of an algorithm in imprecise and imbalanced environment. This methodology was demonstrated on two spot detection algorithms, the LoG-based and wavelets-based methods. It was able to highlight the differences in performance between the two methods. It can be applied on other spot detection algorithms, provided that they seek to find the entire diffraction-limited spot.

REFERENCES

[1] R.D. Larson, H.R. Singer, D. Zenklusen, "A single molecule view of gene expression." Imaging Cell Biology, vol. 19(11), pp. 630–637, 2009.

[2] A. Raj, S.C. Peskin, D Tranchina, D.Y. Vargas, S. Tyagi, "Stochastic mRNA Synthesis in Mammalian Cells." PLoS Biology, vol. 4(10), pp. 1-13, 2006

[3] E.F. DeLong, G.S. Wickham, N.R. Pace, "Phylogenetic stains: ribosomal RNA-based probes for the identification of single cells." Science, vol. 243(4896), pp. 1360-1363, 1989

[4] M. Guttenbach, W. Engel, M. Schmid, "Analysis of structural and numerical chromosome abnormalities in sperm of normal men and carriers of constitutional chromosome aberrations. A review." Human Genetics, vol. 100(10), pp. 1-21, 1997

[5] D.Y. Vargas, K. Shah, M. Batish, M Levandoski, S. Sinha, S.A. Marras, I.P. Schedl, S. Tyagi, "Single-molecule imaging of transcriptionally coupled and uncoupled splicing." Cell, vol. 147(5), pp. 1054-1065, 2011

[6] R.P. Jansen, M Kiebler, "Intracellular RNA sorting, transport and localization." Nat. Struc. & Mol. Bio., vol. 12, pp. 826-829,2005

[7] Y.D. Vargas, A. Raj, S.A.E. Marras, F.R. Kramer and S.Tyagi, "Mechanism of mRNA transport in the nucleus." PNAS, vol. 102(47), pp. 17008-17013, 2005

[8] F.J. Oborra, D.A. Jackson, P.R. Cook, "The path of transcripts from extra-nucleolar synthetic sites to nuclear pors: transcripts in transit are concentrated in discrete structures containing SR proteins." Journal of Cell Science, vol. 115(15), pp. 2269-2282, 1998

[9] C.S. Osborne, L. Chakalova, K.E. Brown, D. Carter, A. Horton, "Active genes dynamically colocalize to shared sites of ongoing transcription." Nature Genetics, vol. 36, pp. 1065-1071, 2004

[10] J.G Bauman, J. Wiegent, P. Borst and P. Duijn, "A new method for fluorescence microscopical localization of specific DNA sequences by in situ hybridization of fluorochrome-labelled RNA." Expe. Cell Research, vol. 128(2), pp. 485-490, 1980

[11] P.R. Langer, A.A. Waldrop and D.C. Ward, "Enzymatic synthesis of biotin-labeled polynucleotides: novel nucleic acid affinity probes." PNAS, vol. 78(11), pp. 6633-6637, 1981

[12] J. Wiegant, T. Ried, P.M. Nederlof, M. van der Ploeg, H.J. Tanke and A.K. Raap, "In situ hybridization with fluoresceinated DNA." Nucleic Acids Research, vol. 19(12), pp. 3237-3241, 1991

[13] R.C. Singer and D.C. Ward, "Actin gene expression visualized in chicken muscle tissue culture by using in situ hybridization with a biotinated nucleotide analog." PNAS, vol. 79(23), pp. 7331-7335, 1982

[14] M. Batish, A. Raj and S. Tyagi, "Single Molecule Imaging of RNA In Situ. Jeffrey E. Gerst (ed.)," RNA Detection and Visualization: Methods and Protocols. Methods in Molecular Biology, vol. 714(1), pp. 3-13,2011

[15] J.B. Lawrence, R.H. Singer, C.A. Villnaye, J.L. Stein, and G.S. Stein, "Intracellular distribution of histone mRNAs in human fibroblasts studied by in situ hybridization." PNAS vol. 85(2), pp. 463-467,1988

[16] A.M. Femino, F.S. Fay, K Fogarty and R.H Singer, "Visualization of single RNA transcripts in situ." Science, vol. 285(5363), pp. 585-590, 1998

[17] A.M. Femino, K.Fogarty, L.M. Lifshitz, W.Carrington, R.H. Singer, "Visualization of single molecule of mRNA in situ." Methods in Enzymology, vol. 361, pp.245-304, 2003

[18] J.M. Levsky, S.M. Shenoy, R.C. Pezo and R.H. Singer, "Single cell gene expression profiling." Science, vol. 297, pp. 836-840, 2002

[19] A. Raj, P. van den Bogaard, S.A. Rifkin, A. van Oudenaarden, S. Tyagi, "Imaging individual mRNA molecules using multiple singly labelled probes." Nature Methods, vol. 5, pp. 877-879, 2008

[20] J.C.Olivo-Marin, "Extraction of spots in biological images using multiscale products." Pattern Recognition, vol. 35, pp. 1989-1996, 2002

[21] T. Trek, A.J. Chao, R.D. Larson, H.Y. Park, D. Zenklusen, M.S. Shenoy, R.H. Singer, "Single-mRNA counting using fluorescent in situ hybridization in budding yeast." Nature Protocols, vol. 7, pp. 408-419, 2012

[22] D. Huttenlocher, G. Klanderman and W. Rucklidge, "Comparing images using the Hausdorff distances." IEEE Trans. Pattern Anal. Machine Intell., vol.15(9), pp. 850-863, 1993

[23] V. Chalana and Y. Kim, "A methodology for evaluation of boundary detection algorithms on medical images." IEEE Trans. Med. Imag., vol. 16(5), pp. 642-652, 1997

[24] T. Landrebe, P. Paclik, D.M.J. Tax, S. Verzakov and R.P.W Duin, "Cost-based classifier evaluation for imbalanced problems." Lecture Notes in Computer Science, vol. 3138, pp. 762-770, 2004

[25] T. Landrebe, P. Paclik, R.P.W. Duin, A.P. Bradley, "Precision-recall operating characteristic (P-ROC) curves in imprecise environments." 18th Inter. Conf. on Pattern Recognition, pp. 123-127, 2006

V. SUPPLIMENTARY DATA

Methods and Materials

The eGFP gene sequence was found on PubMed and inserted in 5'-3' direction into the probe designer algorithm on www.singlemoleculefish.com. The parameters set on the algorithm were as follows:

Number of probes	48
Probe length	20 nucleotides
GC content	45%

No of GFP probes

Lyophilized probes (Biosearch Technologies) were resuspended in 100 µl of TE (10mM Tris, 1 mM EDTA, Sigma) buffer (pH 8) to a final concentration of 100 mM each and stored at -20°C. Equal volumes of thawed probes were aliquoted (10 mM each) and pooled together for each gene to a final concentration of 480 mM for genes with 48 probes. Initially, precipitation was carried out with 10% volume of 3M Sodium Acetate (pH 5.2, Sigma) and 2.5X volume 100% cold Ethanol (Minema) according to smFISH protocol by Batish *et*

al. (2011) Probes were precipitated overnight by incubation at -20°C. Probes were then spun at 14 500 Xg, 4°C for 20 min. The pellet was then resuspended in 200 µl 0.1 M Sodium Bicarbonate (Sigma) or Sodium Tetraborate (Sigma). Approximately 0.3 mg of ATTO-565 NHS-ester dye (ATTO-TEC, Germany) was dissolved in 10 µl dimethyl sulphoxide (DMSO, Sigma). Dissolved dye solution was added to 190 µl of 0.1 M Sodium Bicarbonate (Sigma). The dye solution was added to the probe solution and incubated overnight in the dark at 37°C. Following conjugation reaction, the probes were reprecipitated at -20°C overnight as previously described. Probes were then spun at 14 500 Xg, 4°C for 20 min. Supernatant which consisted of unconjugated dye was discarded and conjugated probe pellet was rinsed twice with 70% Ethanol at 14 500 Xg, 4°C for 5 min. Supernatant was discarded and pellet was allowed to air dry. Pellet was resuspended in 200 µl of Buffer A (0.1 M Triethyl ammonium (TEA, Sigma)). Conjugated probes were separated and purified to enrich for dye-conjugated probes by reverse phase HPLC on a C18 column. Buffer A is the aqueous phase column which allows sample molecules to adhere to column and Buffer B (Triethyl ammonium and 70% (v/v) acetonitrile (Labscan) contains organic solvents in which oligonucleotides are preferentially soluble. An optimized programme of 2 to 98% Buffer B over 20 min was used to purify probes. Conjugated probes were detected at two wavelengths, 260 nm for nucleic acid and corresponding wavelength for dye used either 565 nm for ATTO-565. The appropriate fractions, containing conjugated were collected and dried in a Centri-Vac. Dried probes will were then re-precipitated overnight as previously described. Probes were then spun down with the same parameters as previously described. Probes were allowed to air dry and were re-suspended in a small volume of TE buffer (pH 8, Sigma). DNA concentrations were then determined using a Nanodrop. Probes were then diluted to a final concentration of 50ng and stored at -20°C until hybridization steps.

Cell Culture

Transfections

HeLa cells were grown in DMEM (Dulbecco's Modified Eagles's Medium, Gibco) with 10% FBS (Fetal Bovine Serum, Gibco), 2 mM L-glutamine (Sigma Aldrich) and G418. Cells were transfected with 1 µg JOMU WT and LIpofectamine 2000 (Invitrogen) complexes and 1ml Opti-MEM I Reduced Serum Medium (Gibco). Media was changed to DMEM after 4 hours and cells were incubated at 37°C and 5% CO_2 for 24 hr. Cells were passaged at 1:10 into fresh growth medium containing kanamycin sulphate (Roche). After cells had reached 90% confluency, cells were seeded in 12 well plates, each well containing an ethanol cleaned 15mm coverslip. Approximately 1 X 10^5 cells were seeded in each well in 1 ml of media. Cells were grown in a 37°C incubator with 5% CO_2 overnight. Cells were stimulated with 20ng/ml TNF-α (Tumor Necrosis Factor Alpha, Sigma Aldrich) and fixed after the following time points: 2hr, 2hr 30min and 3hr.

Cell Fixation

For fixation, culture medium was aspirated off wells and cells were gently washed 2X with phosphate buffered saline (PBS, Lonza). 1ml of paraformaldehyde (PFA, Sigma Adrich) was added to cells and incubated in PFA for at least 10min. PFA was aspirated off and cells were gently washed 2X with PBS. Cells were then stored in 70% Ethanol (Minema) at 4°C in parafilm sealed plates until hybridization experiments.

Probe hydrization and Imaging

Prior to hybridization, cells are gently washed 2X with PBS. A volume of 50ng of a specific conjugated probe is then added to hybridization buffer (50% (v/v) deionised formamide (CalBiochem), 10% (w/v) dextran sulphate (Sigma), 300 mM NaCl (Sigma), 20 mM NaH_2PO_4 (Sigma), 2 mM EDTA (Sigma), 10 µl vanadyl ribonucleoside complex (Sigma), 250 ug/ml E. coli tRNA (Sigma). For each coverslip, 7 µl of hybridization buffer containing 50ng of probe is used. Coverslips are then inverted, cell side down, onto 7 µl of hybridization buffer on parafilm coated glass. Hybridization was then carried out in 37°C water bath in the dark overnight. Coverslips were transferred into a 12 and 2X SSC (300 mM

NaCl, 0.3 M tri-sodium citrate, Ambion) at 37°C for 30min. Wash step was repeated three times in fresh wash buffer. Then 0.125 µg DAPI (Invitrogen) was added 20 min into the final wash step and incubated under the same conditions for 10 min. Coverslips were then gently washed 2X in PBS and incubated with equilibration buffer for 2-5min. Coverslips were then mounted onto ethanol cleaned coverslips, using glox buffer containing 3.7 X 10-3 mg/µl glucose oxidase (Sigma) and 164.38U/µl catalase (Sigma) as a mounting buffer. Cells were imaged on a Nikon widefield TIRF microscope using a 100X oil immersion objective under lamp illumination. Imaging was done using mercury lamp illumination through the appropriate filter sets at low camera gain in each of the fluorescent channels using an Andor iXion897 camera. The DAPI nuclear stain was visualized in the 405 channel at 10ms exposure time. GFP was imaged in the 488 channel with 100ms exposure time. eGFP mRNA ("spots") were imaged in the 561nm channel after 200ms exposure (imaging software, µManager).

JOMU WT Plasmid Map